

DIRECT NUMERICAL SIMULATION OF A LAMINAR SEPARATION BUBBLE ON A NACA-0012 AIRFOIL

Lloyd E. Jones, Richard D. Sandberg, Neil D. Sandham
Aerodynamics and Flight Mechanics Research Group,
School of Engineering Sciences
Southampton, England
ljones@soton.ac.uk

ABSTRACT

Direct numerical simulations (DNS) of a laminar separation bubble on a NACA-0012 airfoil at $Re_c = 5 \times 10^4$ and incidence 5° are presented. Initially volume forcing is introduced in order to promote transition. After obtaining sufficient data from this forced case, the explicitly added disturbances are removed and the simulation run further. Upon removal of disturbances, the turbulence is observed to 'self-sustain', and does not decrease in intensity. The forced and unforced cases are then compared, in order to investigate the dependency of bubble behaviour on the addition of disturbances. The results imply that forcing may potentially be used as a control measure to improve aerodynamic performance. Finally, a simplified DNS is presented that illustrates a mechanism for the self-sustaining turbulence that is observed, with implications for separation bubble modelling.

INTRODUCTION

Under an adverse pressure gradient a boundary layer may separate, leading to reverse (upstream) fluid flow. Within the separated region disturbances are strongly amplified, typically leading to transition to turbulence. The resultant turbulent flow enhances mixing and momentum transfer in the wall normal direction, and causes the boundary layer to reattach. This system of laminar separation, transition and turbulent reattachment is referred to as a laminar separation bubble (LSB), and is typically associated with flows at low to moderate Reynolds numbers.

When present on an airfoil, laminar separation bubbles have a marked effect upon aerodynamic performance. Drag forces are typically increased, and the presence of a separation bubble may affect stall behaviour (Gault, 1957). The phenomenon of bubble bursting, where a small increase in incidence leads to a sudden increase in bubble length, causes a dramatic loss in aerodynamic performance and hence is an important consideration in low Reynolds number airfoil design.

Using the results of Gaster (1967), Horton (1969) was the first to describe the time-averaged structure of a laminar separation bubble, and proposed an empirical model for predicting bubble behaviour. Despite refinements such as the use of the e^n transition prediction method, modelling of low Reynolds number effects and the dependency on background turbulence levels, present day models do not adequately predict bubble bursting or unsteady behaviour.

More recently, advances in understanding of laminar separation bubbles have been made via numerical methods. The first numerical studies of separation bubbles were limited

either to 2D analysis (Pauley *et al.*, 1990), or else only studied primary/linear instability and did not resolve transition (Pauley, 1994; Rist, 1994). The first studies to fully resolve transition to turbulence within a laminar separation bubble were conducted by Alam & Sandham (2000), and Spalart & Strelets (2000).

Alam & Sandham (2000) found that reverse flow greater than 15% would be required in order to sustain absolute instability, compared to an observed reverse flow of only 4-8%. As a result, it was concluded that the transition process was driven by convective instability. Spalart & Strelets (2000) conducted DNS of a laminar separation bubble for the purpose of assessing turbulence models. No unsteadiness was introduced and inflow disturbances were less than 0.1%, however transition to turbulence was still observed. As a result the study stated that entry-region disturbances (referring to Tollmien-Schlichting, or TS, type waves) could be discarded as the mechanism behind transition, however the study also stated that magnitude of reverse flow present was unlikely to be sufficient to sustain absolute instability. Hence the first two fully resolved DNS of laminar separation bubble apparently observed different instability mechanisms leading to transition, and different transitional behaviour.

Marxen *et al.* (2003) performed a combined DNS and experimental study of a LSB on a flat plate. Periodic 2D disturbances were introduced upstream of separation, and three-dimensionality was introduced via a spanwise array of spacers. The separated shear layer again was observed to roll up to form vortices which subsequently broke down to turbulence. The same configuration was studied further by Lang *et al.* (2004) and again by Marxen *et al.* (2004) in order to quantify the respective roles of 2D and 3D disturbances. Marxen *et al.* concluded that transition was driven by convective amplification of a 2D TS wave, which also determined the length of the bubble, and that the dominant mechanism behind transition is an absolute secondary instability in a manner first proposed by Maucher *et al.* (1997).

With continued advances in computing power, it is now possible to perform DNS of laminar separation bubbles on full airfoil configurations. This contrasts with previous numerical studies, which have been limited to bubbles on flat plates or other simplified geometries in order to reduce the computational cost. The advantage of studying full airfoil configurations is that the bubble can interact with the potential flow in a coupled fashion, as opposed to subjecting the bubble to pre-determined flow conditions. The bubble will be closer in nature to those observed under flight conditions, and the influence of the bubble behaviour on the aerodynamic performance of the airfoil can be observed directly.

The purpose of the current study is to investigate the dependency of bubble behaviour on the presence of boundary layer disturbances, and to investigate the role of instability mechanisms in separation bubble transition. First, data from three simulations of a laminar separation bubble on a NACA-0012 airfoil will be compared. Then a computationally inexpensive simulation will be presented, intended to explain the self-sustaining turbulence observed in the first part of the study.

NUMERICAL METHOD

Simulations were run at a Reynolds number based on airfoil chord of $Re_c = 5 \times 10^4$, and Mach number $M = 0.4$. All cases were run at five degrees incidence with a constant timestep of $\Delta t = 1 \times 10^{-4}$. The DNS code directly solves the unsteady, compressible Navier-Stokes equations, written in non-dimensional form as

$$\frac{\partial \rho}{\partial t} + \frac{\partial \rho u_i}{\partial x_i} = 0 \quad (1)$$

$$\frac{\partial \rho u_i}{\partial t} + \frac{\partial \rho u_i u_j}{\partial x_j} + \frac{\partial p}{\partial x_i} = \frac{\partial \tau_{ij}}{\partial x_j} + F_i \quad (2)$$

$$\frac{\partial \rho E_t}{\partial t} + \frac{\partial}{\partial x_i} (\rho E_t + p) u_i = - \frac{\partial q_i}{\partial x_i} + \frac{\partial u_i \tau_{ij}}{\partial x_j} \quad (3)$$

where F_i is a forcing term used in simulation 3DF, defined later, and E_t is the total energy per unit volume defined as

$$E_t = \frac{T}{\gamma(\gamma - 1)M^2} + \frac{1}{2}(uu + vv + ww) \quad (4)$$

The stress terms τ_{ij} are defined as

$$\tau_{ij} = \frac{\mu}{Re} \left(\frac{\partial u_i}{\partial x_j} + \frac{\partial u_j}{\partial x_i} \right) - \frac{2}{3} \frac{\mu}{Re} \frac{\partial u_k}{\partial x_k} \delta_{ij} \quad (5)$$

and conduction term q_i is defined as

$$q_i = \frac{-\mu}{(\gamma - 1)M^2 Re Pr} \frac{\partial T}{\partial x_i} \quad (6)$$

Viscosity is calculated using Sutherlands law (White, 1991), and finally the perfect gas law, $p = \rho T / \gamma M^2$, relates p , ρ and T .

The primitive variables ρ, u, v and T have been non-dimensionalised by the freestream conditions and the airfoil chord is used as the reference length scale. Dimensionless parameters Re, Pr and M are defined using free-stream (reference) flow properties. The ratio of specific heats is specified as $\gamma = 1.4$ and the Prandtl number as $Pr = 0.72$.

Fourth order accurate central differences utilising a five-point stencil are used for the spatial discretisation. Fourth order accuracy is extended to the domain boundaries by use of a Carpenter boundary scheme (Carpenter *et al.*, 1999). No artificial viscosity or filtering is used. Instead, stability is enhanced by appropriate treatment of the viscous terms in combination with entropy splitting of the inviscid flux terms (Sandham *et al.*, 2002). The explicit fourth order accurate Runge-Kutta scheme is used for time-stepping.

The code is based upon an existing code that has been previously validated for compressible turbulent plane channel flow (Sandham *et al.*, 2002), and more recently has been demonstrated to accurately represent the development of hydrodynamic instabilities (Sandberg *et al.*, 2007). The code used in the current study is different in that it is applied to a curvilinear C-type grid with wake connection, however

Table 1: Grid parameters

N_ξ	N_η	N_z	N_{total} (3D)
2570	692	96	1.71×10^8

the same metric terms were used in previous versions of the code.

The topology of the curvilinear C-grid used is given in figure 1. The chosen airfoil geometry is a NACA-0012 airfoil, extended to include a sharp trailing edge and rescaled to unit chord length. The coordinate system is defined such that the trailing edge is located at $(x, y) = (1, 0)$. The spanwise domain width in 3D simulations is 0.2, unless otherwise stated.

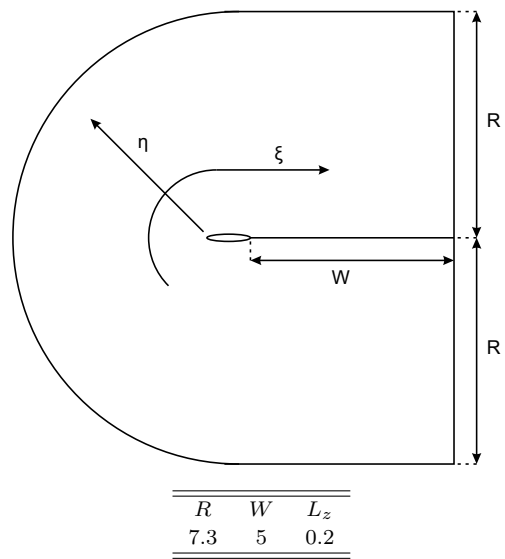


Figure 1: Topology of the computational domain, dimensions listed.

Grid generation for high-order non-dissipative codes is non-trivial, and achieved by an iterative approach. The presence of under-resolved flow phenomena results in numerical oscillations, particularly in sensitive quantities such as density gradient. By analysing simulation results, locations of poor resolution may be identified by such oscillations. A new grid is then generated, with the purpose of improving the resolution in the necessary locations, and the flow-field data interpolated onto the new grid. The simulation is then run on the new grid and the results analysed in order to assess whether resolution issues have been eliminated. The process is repeated as often as necessary, and avoids the need for starting simulations from scratch. All simulations presented used the same grid, with specifications given in table 1.

At the freestream (η^+) boundary, where the only disturbances likely to reach the boundary will be in the form of linear waves, an integral characteristic boundary condition is applied (Sandhu & Sandham, 1994). At the downstream exit boundary (ξ^\pm), which will be subject to the passage of nonlinear fluid structures, a zonal characteristic boundary condition (Sandberg & Sandham, 2006) is applied for increased effectiveness. At the airfoil surface an adiabatic, no slip condition is applied.

Volume forcing is applied to the x and y momentum equations in the 3D simulation, the goal being to intro-

Table 2: Forcing parameters.

ω	β
48.76	31.42
53.60	94.24
53.60	125.66

duce oblique disturbances that are amplified in the free-shear layer and subsequently break down to turbulence. Forcing is applied about the location $x = 0.1, y = 0.129$, corresponding to a point within the boundary layer of the time-averaged solution, and is periodic in both time and span. A cosine function is used to smoothly ramp the forcing terms from a maximum at the centre of the forcing location to zero at radius 5×10^{-3} from the forcing location. Frequencies were chosen based on linear stability analysis of the 2D time averaged flowfield, selecting the most unstable modes observed. Forcing was applied at several spanwise wavenumbers, with the total amplitude 0.1% of the freestream velocity. Details of forcing parameters are given in table 2, where $\omega = 2\pi f$, with f the frequency, and β the spanwise wavenumber.

DNS OF A LAMINAR SEPARATION BUBBLE

Results from three DNS will be presented, defined as follows.

Case 2D: A precursory 2D simulation that was run in order to provide a suitable initial condition for the subsequent 3D simulation.

Case 3DF: The 2D flowfield was extruded in the z -direction and three-dimensionality was introduced by explicitly adding disturbances via volume forcing. The goal is to excite unstable oblique modes which would subsequently be amplified within the separated shear layer, leading to transition to turbulence.

Case 3DU: After an appropriate amount of statistical data was captured from case 3DF, the simulation was progressed further in time with the explicitly added forcing removed. The dependency of bubble behaviour on the addition of disturbances could then be investigated.

Time dependent behaviour

In 2D, the time dependent lift coefficient (C_L) exhibits periodic oscillatory behaviour with frequency $f = 3.37$ and $(C_L)_{RMS} = 0.0172$. Iso-contours of vorticity (figure 2, top) illustrate the cause of this behaviour. The boundary layer on the upper airfoil surface is observed to separate near the leading edge, and subsequently rolls up into vortices which then convect downstream, as observed by Marxen *et al.* (2003) in flat plate simulations. The periodic vortex shedding results in the observed periodic oscillation in C_L and C_D .

Figure 3 shows a time-history of C_L and C_D starting at time $t = 0$, the start of case 3DF. The time dependent C_L initially displays oscillatory behaviour associated with 2D vortex shedding. This oscillatory behaviour ceases by time $t = 2$, whereupon C_L increases significantly. At this stage in the flow development, time series of pressure taken within the separated shear layer (figure 4, $x = 0.4$) clearly exhibit periodic oscillation, associated with the strongly amplified instability waves induced by the forcing. Downstream of the vortex shedding location, at $x = 0.8$, the pressure signal is seemingly random, characteristic of turbulent fluctuations passing the measurement location. Instantaneous

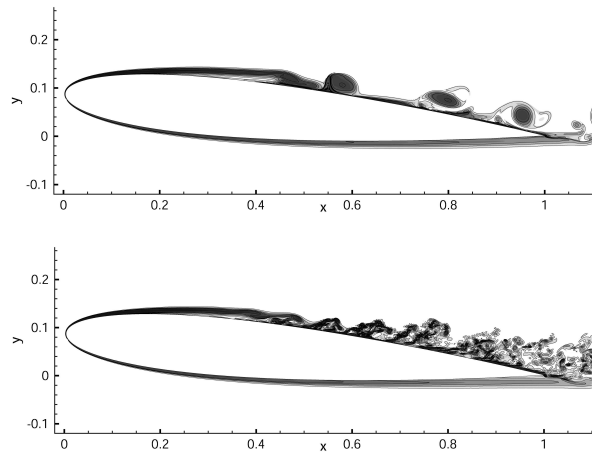


Figure 2: Iso contours of vorticity using 10 levels over the range ± 150 for both the 2D case (top), and case 3DF (bottom), taken at mid-span.

iso-contours of vorticity taken at the mid-span (figure 2, bottom) illustrate that the separated shear layer undergoes transition to turbulence, and that a developing turbulent boundary layer is now present over the aft section of the airfoil. Iso-surfaces of the secondary invariant of the velocity gradient tensor, Q , illustrate structures present in the transition region (figure 5, top). Structures within the boundary layer are observed to break down to smaller scales, however no large-scale Λ -vortices are observed here. After a transient lasting until approximately $t = 6.3$, case 3DF settles to a stationary flow and statistics were taken for $6.3 < t < 14$. Figure 3 illustrates the data capture period for both 3D simulations.

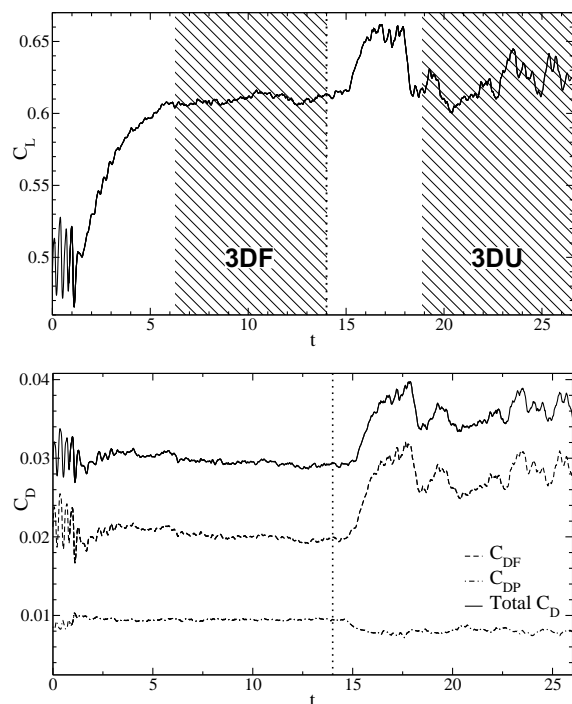


Figure 3: Time dependent lift (top) and drag (bottom) coefficients for the 3D cases. The dotted line indicates the time at which forcing was removed ($t = 14$). Hatched areas indicate periods over which statistical data capture was undertaken.

Table 3: Time averaged lift and drag coefficients for all cases.

Case	C_L	C_D	C_{DF}	C_{DP}
2D	0.499	0.0307	0.0087	0.0220
3DF	0.621	0.0294	0.0095	0.0199
3DU	0.615	0.0358	0.0081	0.0278

Case 3DF was then run further in time but with the explicitly added forcing removed, and the resultant simulation denoted 3DU (3D unforced). Upon removing the forcing, the turbulent behaviour can be monitored by observing pressure fluctuations within the boundary layer (figure 4). It can be seen that downstream of the separation bubble, at $x = 0.8$ the pressure fluctuations do not decrease. In fact, the maximum amplitude of pressure fluctuations increases slightly. Oscillations are still observed within the separated shear layer at $x = 0.4$, however the signal is lower in amplitude, more intermittent, and no longer dominated by the forcing frequencies as observed in case 3DF. Statistics for case 3DU were taken for $18.9 < t < 26.6$. At the end of this period of time turbulent fluctuations have still not decreased in amplitude, and the turbulence appears to self-sustain. Iso-surfaces of Q illustrate structures present in the transition region (figure 5, bottom). In contrast to the forced case, much larger structures may be observed, with clear spanwise orientation. These structures persist downstream of the transition region of case 3DF, until they break down into turbulence with strong spanwise coherence. Animations of flowfield properties suggest that the transition process is highly erratic.

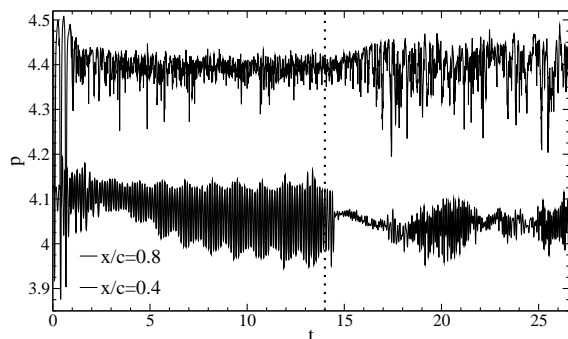


Figure 4: Time dependent pressure within the boundary layer at $x = 0.4$ (lower curve) and $x = 0.8$ (upper curve). The dotted line indicates the time at which forcing was removed.

Statistical analysis

Time dependent lift and drag coefficients are given in figure 3, and resultant time averaged values are given in table 3. It can be seen that whilst removal of forcing leads to a slight increase in C_L and a very slight decrease in friction drag (C_{DF}), pressure drag (C_{DP}) is subject to a significant increase. The net effect is to decrease L/D from 21.1 to 17.2., hence it appears that the presence of forcing improves the aerodynamic performance of the airfoil.

Time averaged pressure coefficient (C_p) distributions are plotted for all cases in figure 6. In all cases a pronounced pressure plateau is visible on the upper airfoil surface, illustrating the presence of a separation bubble. Comparing cases 3DF and 3DU, it can be seen that the length of the

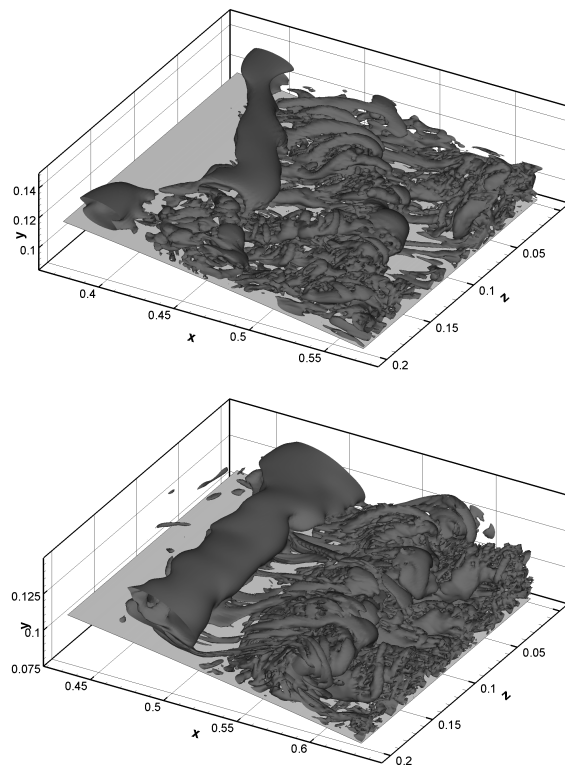


Figure 5: Iso-surfaces of the second invariant of the velocity gradient tensor at $Q = 500$, for case 3DF (top) and case 3DU (bottom).

Table 4: Time averaged separation and reattachment points.

Case	x_{sep}	x_{reatt}
2D	0.151	0.582
3DF	0.133	0.504
3DU	0.099	0.607

pressure plateau has increased significantly in the unforced case, whereas downstream of the bubble the C_p distributions are similar. The slight C_L increase in case 3DU can be attributed to the increased length of the pressure plateau. The increase in C_{DP} for case 3DU can also be attributed to the increase in length of the pressure plateau, since pressure recovery is delayed downstream of the point of maximum airfoil thickness.

Time averaged skin friction coefficient (c_f) distributions (figure 6) give a quantitative measure of bubble length (table 4). Comparing the 2D simulation to case 3DF it can be seen that the bubble length has decreased in the 3D case. Due to the presence of transition to turbulence and hence increased wall normal mixing, the reattachment point has moved upstream from $x = 0.582$ to $x = 0.504$. The separation point has also moved upstream slightly in the forced 3D case. Comparing the two 3D cases, it can be seen that removing the forcing has increased the bubble length significantly. The reattachment point has moved from $x = 0.504$ in case 3DF to $x = 0.607$ in case 3DU. The c_f peak downstream of transition decreases upon removal of forcing, resulting in the slight decrease in C_{DF} observed in case 3DU.

Iso contours of turbulent kinetic energy, defined as $K = \frac{1}{2}(\overline{u'u'} + \overline{v'v'} + \overline{w'w'})$, show a significant increase in peak K upon removal of forcing (increasing from 0.074 to 0.124),

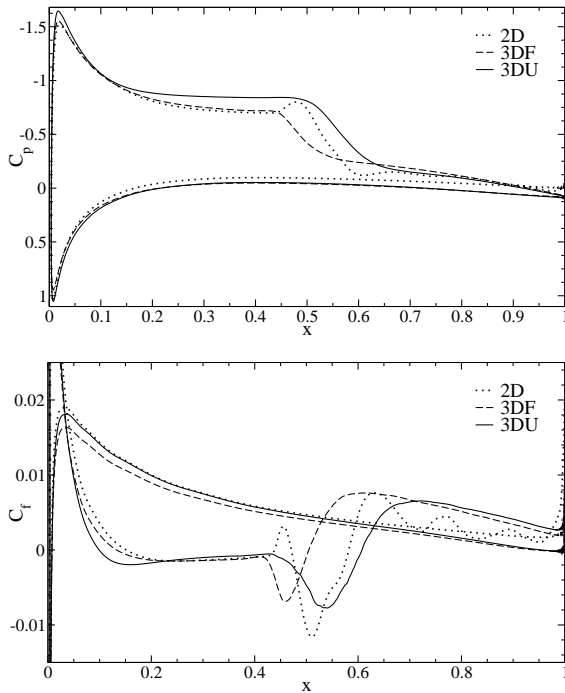


Figure 6: Time averaged distributions of C_p (top) and c_f (bottom) for all three cases.

thus it appears the transition process in the forced case is more energetic than in the forced case. In case 3DU the peak K occurs upstream of the time-averaged reattachment point, whereas in case 3DF the peak K occurs in the direct vicinity of reattachment, which may explain why the peak c_f is lower in case 3DU (figure 6).

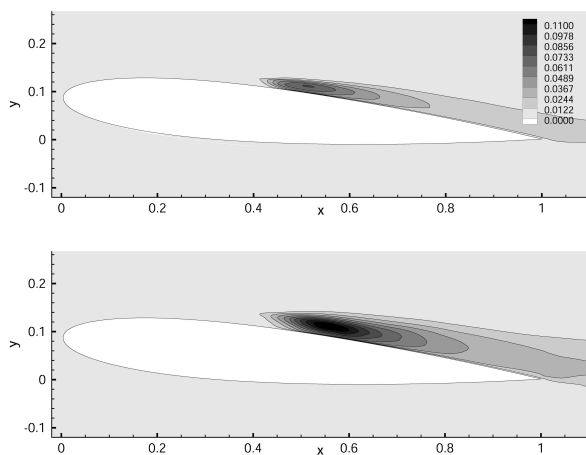


Figure 7: Iso contours of K for case 3DF (top) and 3DU (bottom), using 20 levels over the range 0 to 0.11.

It is important to note that upon removal of forcing the bubble properties do not tend toward 2D behaviour. If the bubble were purely convectively unstable, one would expect turbulent fluctuations to convect downstream and ultimately leave the flow over the airfoil in an unperturbed state. This is clearly not the case, and some other mechanism must be present in order for the turbulence to self-sustain.

A MECHANISM FOR SELF SUSTAINING TURBULENCE

Linear stability analysis of the time averaged flowfield has been performed for case 3DF and case 3DU, using an incompressible Orr-Sommerfeld solver in conjunction with the cusp-map method for determining the presence of absolute instability (Schmid *et al.*, 2002). For both cases, the separated shear layer was found to be convectively unstable from $x = 0.1$ up to and beyond the region of maximum reverse flow. No evidence of absolute instability was observed. However, the persistence of turbulence upon removal of forcing suggests that some mechanism other than convective disturbance growth is present. A series of computationally inexpensive simulations were therefore conducted, in order to determine whether any instability mechanism is present in the current case that is not predicted by simple linear stability theory.

A 3D simulation is initialised in the same manner as case 3DF. A small number of spanwise points (16) are used, over a narrow spanwise domain ($L_z = 0.135$). No time periodic forcing is added, but w -perturbations are superposed onto the initial condition in the form of white noise. The w -perturbations are 1×10^{-8} in amplitude, and only the boundary layer over the upper surface of the airfoil is seeded in this fashion. The simulation is progressed from this initial condition and no further disturbances are added. The stability characteristics of the unsteady 2D separation bubble with vortex shedding may then be determined. The perturbations will either convect downstream whilst decaying or amplifying, ultimately leaving the flow over the airfoil unperturbed, or the perturbations will grow temporally without convecting downstream as in absolute instability.

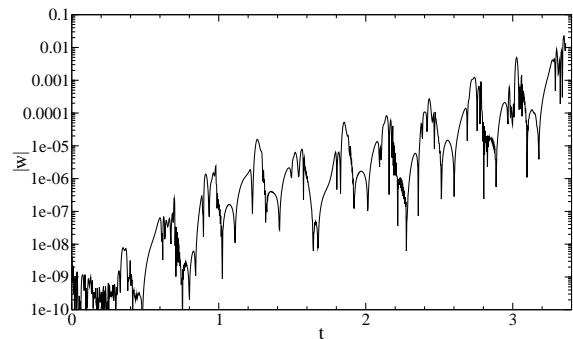


Figure 8: Time series of absolute w velocity taken at a point within the boundary layer at $x = 0.6$.

The resultant behaviour is illustrated by plotting absolute values of w -velocity against time, recorded at $x = 0.6$ within the boundary layer (figure 8). It can be seen that the perturbations do not convect downstream leaving the source unperturbed, but grow in amplitude temporally until nonlinear magnitudes are reached. The behaviour is more clearly illustrated in animations of $|w|$. The w -perturbations grow in amplitude within individual vortices as they convect downstream, however, within the vicinity of the vortex shedding location the perturbations also exhibit growth in amplitude without convecting downstream. Plotting the streamwise vorticity component in the vicinity of the vortex shedding location reveals spanwise periodic structures associated with the instability (figure 9). This behaviour appears qualitatively similar to that proposed by Maucher *et al.* (1997), which was subsequently referred to in the study of Marxen *et al.* (2003) to describe the transition process observed. It appears that the 2D vortex shedding flow is

absolutely unstable to 3D disturbances, in a manner not predictable via linear stability analysis of the time-averaged flowfield. Case 3DF may thus be described as exhibiting transition driven by convective instability, and case 3DU by absolute instability of 2D vortex shedding. It appears that laminar reattachment is not possible for the current case, due to the presence of this absolute instability.

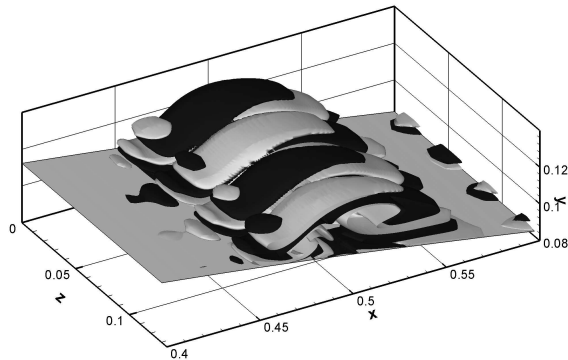


Figure 9: Iso-surfaces of streamwise vorticity taken within the recirculation region at $t = 1.68$ after initialisation, plotted at levels $\pm 2.5 \times 10^{-3}$.

CONCLUSIONS

DNS were conducted of a laminar separation bubble on a NACA-0012 airfoil at five degrees incidence. The 3D separation bubble was found to be highly dependent on the presence of forcing. Compared to the unforced case, the inclusion of forcing increases the L/D ratio by approximately 23% and the intensity of turbulent/unsteady fluctuations over the airfoil are significantly reduced. Forcing in a similar fashion could potentially be used as a control mechanism for improving low Reynolds number airfoil performance. Upon the removal of forcing, the turbulence over the aft section of the airfoil is observed to self-sustain. A 3D simulation, resolving the linear response to 3D perturbations, suggests that the 2D vortex shedding behaviour is absolutely unstable to 3D perturbations in a manner similar to that suggested by Maucher *et al.* (1997). Therefore, in the absence of convectively driven transition within the shear layer, transition will take place by absolute instability of the 2D vortex shedding. This has important implications for the modelling of laminar separation bubbles, suggesting that if freestream turbulence levels drop below a certain value, the time-averaged transition and reattachment locations will be fixed and not vary with further decreases in freestream turbulence levels.

ACKNOWLEDGMENTS

Computer time was provided by the EPSRC grant GR/S27474/01.

REFERENCES

Alam, M. & Sandham, N. D. 2000 Direct numerical simulation of ‘short’ laminar separation bubbles with turbulent reattachment. *J. Fluid Mech.* **403**, 223–250.

Carpenter, M. H., Nordström, J. & Gottlieb, D. 1999 A stable and conservative interface treatment of arbitrary spatial accuracy. *J. Comp. Phys.* **148** (2), 341–365.

Gaster, M. 1967 The structure and behaviour of separation bubbles. Aeronautical Research Council Reports and Memoranda 3595. Aerodynamics Division N. P. L.

Gault, D. 1957 A correlation of low-speed airfoil-section stalling characteristics with Reynolds number and airfoil geometry .

Horton, H. 1969 A semi-empirical theory for the growth and bursting of laminar separation bubbles. Aeronautical research council current paper 1073.

Lang, M., Rist, U. & Wagner, S. 2004 Investigations on controlled transition development in a laminar separation bubble by means of LDA and PIV. *Experiments in Fluids* **36** (1), 43–52.

Marxen, O., Lang, M., Rist, U. & Wagner, S. 2003 A Combined Experimental/Numerical Study of Unsteady Phenomena in a Laminar Separation Bubble. *Flow, Turbulence and Combustion* **71** (1), 133–146.

Marxen, O., Rist, U. & Wagner, S. 2004 Effect of spanwise-modulated disturbances on transition in a separated boundary layer. *AIAA Journal* **42** (5), 937–944.

Maucher, U., Rist, U. & Wagner, S. 1997 Secondary Disturbance Amplification and Transition in Laminar Separation Bubbles. *Institut für Aerodynamik und Gasdynamik, Universität Stuttgart, Germany* .

Pauley, L. 1994 Response of two-dimensional separation to three-dimensional disturbances. *ASME, Transactions, Journal of Fluids Engineering* **116** (3), 433–438.

Pauley, L. L., Moin, P. & Reynolds, W. C. 1990 The structure of two-dimensional separation. *J. Fluid Mech.* **220**, 397–411.

Rist, U. 1994 Nonlinear effects of 2D and 3D disturbances on laminar separation bubbles. *Proceedings of IUTAM Symposium on Nonlinear Instability of Nonparallel Flows. Springer-Verlag, New York* pp. 324–333.

Sandberg, R. D. & Sandham, N. D. 2006 Nonreflecting zonal characteristic boundary condition for direct numerical simulation of aerodynamic sound. *AIAA J.* **44** (2), 402–405.

Sandberg, R. D., Sandham, N. D. & Joseph, P. F. 2007 Direct numerical simulations of trailing-edge noise generated by boundary-layer instabilities. *J. Sound and Vibration* Accepted for publication.

Sandham, N., Li, Q. & Yee, H. 2002 Entropy splitting for high-order numerical simulation of compressible turbulence. *J. Comp. Phys.* **178**, 307–322.

Sandhu, H. & Sandham, N. 1994 Boundary conditions for spatially growing compressible shear layers. *Report QMW-EP-1100, Faculty of Engineering, Queen Mary and Westfield College, University of London* .

Schmid, P., Henningson, D. & Jankowski, D. 2002 Stability and Transition in Shear Flows. Applied Mathematical Sciences, Vol. 142. *Applied Mechanics Reviews* **55**, B57.

Spalart, P. & Strelets, M. 2000 Mechanisms of transition and heat transfer in a separation bubble. *J. Fluid Mech.* **403**, 329–349.

White, F. M. 1991 *Viscous Fluid Flow*. McGraw Hill.